IJAER/ Nov-Dec 2021/Volume-10/Issue-6 ISSN: 2278-9677
International Journal of Arts & Education Research

ACOUSTICAL PROPERTIES OF METAL OXIDE NANOPARTICLES FOR ENERGY STORAGE APPLICATIONS

Sunil Meena

Associate Professor Physics

Government College Bundi (Rajasthan)

ABSTRACT

This paper investigates the effect of metal oxide (MOx) nanoparticles on thermophysical properties of phase change material (PCM) for thermal energy storage applications. Different types of (MOx) nanoparticles include Titanium di-oxide (TiO2), Zinc oxide (ZnO), Ferric oxide (Fe2O3) and Silicon di-oxide (SiO2) were added independently in the magnesium nitrate hexahydrate, an inorganic salt hydrate PCM, to form PCM-metal oxide nanocomposite by melt mixing technique. The scanning electron microscopy was done to investigate the shape and morphology of nanoparticles and their uniform distribution in the PCM matrix. Structural and interaction between nanoparticles and PCM were analyzed by X-ray diffraction (XRD) and Fourier transformed infrared (FTIR) spectroscopic techniques, respectively. The cyclic stability of the prepared nanocomposites was confirmed by thermogravimetric analysis. Nanoparticles concentration in the PCM matrix is very crucial and needs to be carefully optimized to maximize the thermal conductivity enhancement and herein we found that 0.5 wt.% of NPs in PCM matrix show promising thermophysical properties. Thermal conductivity of PCM-metal oxide nanocomposites was improved by 147.5%, 62.5%, 55% and 45% by the addition of 0.5 wt.% TiO2, ZnO, Fe2O3 and SiO2, respectively. The addition of nanoparticles modified the phase change process of PCM nanocomposites and also reduced the phase change temperature range. Besides thermal conductivity enhancement, these also eliminate supercooling while maintain the latent heat capacity. The heat transfer characteristics of PCM-metal oxides nanocomposites were analyzed by conventional heating systems. The PCM-TiO2 nanocomposite demonstrates the best heat transfer characteristics and reduces the phase transition time performances amongst the other metal oxide nanoparticles. It was found that the charging and discharging rate increased by 33% and 77.5% respectively, upon using 0.5 wt.% TiO2 in comparison to pristine PCM and used as a potential material in instant solar water heating system for solar thermal energy storage application.

Keywords: *Acoustical, Metal Oxide, Energy Storage*

INTRODUCTION

In recent times, the rapid development in technologies, commercialization, and industrialization have caused a substantial increment in the requirement of global energy consumption . Fossil fuels are at the top of energy sources despite having a lot of negative issues. Even, according to statistics in 2019, 84% of the total global energy was generated from fossil fuels such as natural gas, coal, and oil. Due to the use of fossil fuels for energy production, several negative impacts are occurring, such as global warming, rise in sea level, soil pollution, water pollution, and air pollution which cause significant harm to flora and fauna. Researchers are working with great concern to minimize the use of such fossil fuels for which they have carried out approaches to utilize renewable sources for the fulfillment of energy requirements. However, the

development of these approaches to utilize renewable sources are not sufficient. Additionally, to utilize green sources it's required to develop efficient energy storage devices so that it can be possibleto use the energy from such storage devices whenever power and energy are required. Nowadays, molten salt nanofluids are used as thermal energy storage (TES) materials for concentrated solar power (CSP) plants for large scale power generation. However, the appropriate synthesizing of molten salt for enhanced specific heat capacity is becoming an obstacle in its application . Electrochemical energy storage is the most popular way to store energy for further use and there are several systems including fuel cells, supercapacitors, and batteries which are applied to store energy thermochemically. Researchers are working towards advancements in energy storage textiles to enhance the wearability and electrochemical performances and stability of batteries, and supercapacitors for improving their applicability for several purposes . Wearable energy storage devices prepared using MO nanosheets can be integrated with bioenergy from biofluids, and bioenergy from human motions, and these integrated mechanisms possess attractive potential for building self-driven body-worn electronic devices . Nano structure-enhanced electrochemical energy storage devices can be integrated with self-operated sensors toward self-sustainable gadgets for the management of health and wellbeing . Due to possessing a high energy density and attractive kinetics, thermochemical energy storage is the preferred system. Fuel cells possess better energy conversion potential than supercapacitors and batteries, but the limitations of fuel cells include a shorter lifespan, less durability, and high cost due to applying several expensive catalysts . Supercapacitors possess higher cyclic stability, better energy, and power density, and better kinetics for charging and discharging than batteries, but these are limited to lower energy density and lower specific capacitanc. To enhance the lifecycle, durability, and stability of the electrode material, the phase transition reaction should have potential reversibility and there should also be a proper space where atomic-level reactions can take place. Therefore, to utilize the concept of electrochemical energy storage (EES), two-dimensional (2D) metal oxide electrodes are one of the best solutions that can increase the cyclic lifetime, power, and energy density of storage devices . Two-dimensional MO nanosheets (MO-NSs) are rapidly emerging due to their applicability in EES devices and their ability to ameliorate performance parameters. Due to the variable valence states of these 2D materials, MO-NSs possess rich redox reactions. This feature assists to improve the storage capacity of suitable electrode materials used in batteries and supercapacitors. Two-dimensional MO nanosheets possess less volume change, more active sites, and less diffusion length compared to metal oxide nanostructures. These features assist to improve the electrochemical energy storage performance by enhancing cycling stability, specific capacity, surface area, and capacitance retention.

Two-dimensional metal oxide nanosheets possess a thickness of only a few atomic thin layers. Compared to 1D and 3D nanostructure materials, they possess several conveniences and limitations. Having a larger surface area is a major convenience of 2D nanosheets that exhibit much more reactivity than 1D and 3D nanostructures, and this feature makes them more promising for energy storage applications, such as fuel cells, supercapacitors, and batteries. These 2D nanosheets are also more suitable in sensors and flexible electronics compared to 1D and 3D nanostructures due to their flexibility feature. However, the high cost of 2D nanosheets is the main barrier to the synthesis and fabrication of these nanosheets and these problems have limited the wide application of 2D metal oxide nanosheets in energy storage systems . Overall, metal oxide (MO) nanosheets possess some uncommon attractive features that make them useful for electrochemical energy storage, but their preparation and manipulation processes may stand as a barrier during application in some cases. Researchers have developed a lot of methodologies to synthesize 2D metal oxide nanosheets using top-down and bottom-up approaches. Figure 1 illustrates the number of publications

on metal oxide nanosheets from 2010 to 2022. The chemical vapor deposition, sol-gel method, and exfoliation with some merits and demerits are the most used approaches by researchers. In the sol-gel approach, a precursor is used to prepare a gel which is further heated to prepare nanosheets. In the case of chemical vapordeposition, the main advantages includes its capability to generate high-quality nanosheet materials with a large surface area. However, its low yield limits its wide application . Exfoliation can also synthesize a massive amount of 2D nanosheets by applying mechanical or chemical intercalation to weaken the interlayer and molecular forces . In recent years, hydrothermal and electrophoretic synthesis approaches have gained much research interest as these methodologies can provide a high yield, as well as good dimensional control .

OBJECTIVE

1. To study on Acoustical Properties of Metal Oxide Nanoparticles for Energy Storage Applications
2. To study on Synthesis of TiO2 nanoparticles

METHOD

Inorganic salt hydrate, magnesium nitrate hexahydrate (Mg (NO3)2•6H2O), isopropyl alcohol (IPA), and titanium tetra isopropoxide were purchased from Alfa Aesar, Germany. Metal oxide NPs (ZnO, Fe2O3, and SiO2) were also purchased from Sigma Aldrich. The supplied materials were used as it is without further purification.

Synthesis of TiO2 nanoparticles

The TiO2 NPs were prepared by the already reported sol-gel method . In this procedure, 20 mL titanium tetra isopropoxide was added dropwise into the 22 ml solution containing 10 ml of isopropanol and 12 ml deionized water under constant stirring at 80 °C for homogenous mixing and then left undisturbed for 1hr. To form the gel, concentrated HNO3 (8 ml) with deionized water as a solvent was added to the above solution. To remove the solvent and residual water, the solution was kept under constant stirring at 60 °C for 2 hrs. resulted in the formation of TiO2 nanoparticles.

Preparation of PCM-metal oxide nanocomposite

The PCM–metal oxide nanocomposite was prepared by melt mixing technique as reported previously . In this procedure, 10 gm of pristine PCM was heated on a hot plate (IKA RCT basic) to its phase transition temperature. The synthesized TiO2 NPs were then added to molten PCM and mixed thoroughly using magnetic stirrer for 20 min to formulate a stable PCM-nanocomposite. Finally, the prepared composite was ultrasonicated (Telesonic, Ultrasonics) for 15 min to obtain a homogeneous dispersion of PCM-TiO2 nanocomposite. The TiO2 NPs with different weight fractions ranging from 0.2–1 wt.% were used to prepare different PCM-nanocomposites. According to our experiments, we found that the optimal mass fraction of TiO2 nanoparticles is 0.5 wt. % for the preparation of stable PCM-nanocomposite. The other metal oxides nanoparticles such as ZnO, Fe2O3, and SiO2 were used for the preparation of other PCM-Metal oxide nanocomposites, with 0.5 wt.% concentration. These PCM-nanocomposites were used for comparative study with TiO2 NPs based PCM nanocomposite.

Characterizations

The morphology and size measurements of materials were done using the scanning electron microscope (SEM), on a Zeiss (EVO-18). The SEM micrographs were used to evaluate the shape and size of synthesized TiO2 and other metal oxides NPs and to observe their dispersion in the PCM composite matrix. The presence of nanoparticles in PCM matrix was also confirmed by EDX analysis (Oxford Instruments). The crystalline phase of all metal oxide embedded-PCM nanocomposites was examined by X-ray diffraction technique (XRD D8ADAVNCE, BRUKER). The interaction between PCM (magnesium nitrate hexahydrate) and the nanoparticles was investigated by Fourier transformed infrared spectrophotometer (FTIR, VERTEX 70 BRUKER). Thermal properties such as latent heat, melting and solidification temperature were measured with Differential scanning calorimeter (DSC, NETZSCH) at a constant heating rate of 5 °C/min, in the temperature range of 30 °C to 120 °C in nitrogen atmosphere. In addition to this measurement, the thermal stability of PCM-nanocomposite was further tested by Thermogravimetric analysis (TGA) from room temperature to 600 °C at a heating rate of 10 °C/min, in nitrogen atmosphere using TA Q500 Instrument. The thermal conductivity of various PCM nanocomposites samples was measured by using a Linseis Transient Hot Bridge-Thermal conductivity meter (THB6N43) under standard laboratory conditions. This instrument works on the principle of hot disk technique, in which the sensors were sandwiched between two samples having parallel plane surfaces to ensure good contact between the sensor and material. To investigate the transient heat transfer characteristics during the melting and solidification of PCM-nanocomposite, a conventional heating, and solar illumination experimental setup, was used as reported previously . The 10 sets of experiments were performed under each condition

RESULT AND DISCUSSION

Morphological and structural analysis

The SEM images were taken to understand the surface morphology of metal oxides NPs and PCM-nanocomposites. The SEM images of TiO2 and other metal oxides nanoparticles (ZnO, Fe2O3, and SiO2) are shown in [Fig. 1(a) and Fig. S1(a-c)] respectively. The as-prepared TiO2 NPs are found to have a spherical morphology with uniform shape and size having an average particle size of 50 nm. The average particle size of the other metal oxide NPs such as ZnO, Fe2O3, and SiO2 is 115 nm, 84 nm, and 130 nm, respectively. The surface morphology of solid pristine PCM is also shown in Fig. 1(b). The TiO2 NPs embedded in PCM micrograph are shown in Fig. 1(c) clearly reveals that the resultant PCM nanocomposite has smooth surface and particles are well dispersed in PCM matrix. The Fig. S2(a-c) shows the SEM image of other PCM-metal oxides (ZnO, Fe2O3, and SiO2) nanocomposites also depicts that the particles are less uniformly dispersed in comparison to TiO2 NPs in PCM matrix and nanocomposite have less smooth surface in comparison to the PCM-TiO2 nanocomposite. The non-uniformity and less smooth surface can be attributed to the larger size of other metal oxides NPs in PCM matrix. In order to investigate the elemental presence of NPs in PCM matrix, EDX analysis was done. The EDX spectrum of PCM-TiO2 nanocomposite depicted in Fig. 1(d) clearly shows respective peaks of Mg, N, O, and Ti mainly from magnesium nitrate hexahydrate and TiO2 nanoparticles. However, the EDX spectrum as shown in Fig. S3(a-c) for other PCM-metal oxide nanoparticles such as (ZnO, Fe2O3, and SiO2) shows the similar peaks Mg, N, O, Zn, Fe, and Si mainly from PCM and nanoparticles respectively clearly confirms the formation of PCM-nanocomposites. No other peaks related to impurities are present in the EDX spectra. To investigate the interaction between PCM and TiO2 NPs in PCMnanocomposite, the FTIR measurement was done in the wavenumber range of 4000–500 cm−1 as shown in Fig. 2. The FTIR spectrum of pristine PCM shows characteristic peaks for OeH stretching

at 3400 cm−1 , N O bending at 1550 cm−1 , a mixture of NeO stretching and bending of N=O at 1300 cm−1 , plus a sharp peak at 819 cm−1 for NO3 − cm−1 which are in good agreement with the reported FTIR spectrum of MNH [24]. In the spectrum of (Mg (NO3)2•6H2O) - TiO2 nanocomposite, no new peaks or shift is observed with respect to pristine PCM. This indicates that there is no chemical interaction between TiO2 NPs and the PCM.

The measured FTIR spectrum of PCM-ZnO, PCM-Fe2O3, and PCMSiO2 nanocomposite is also shown in Fig. S4(a-c) and show similar behavior as shown in Fig. 2. Thus NPs are physically mixed to form a PCM-nanocomposite in all the samples under investigation. Similar FTIR results were reported by other groups which confirms a simple physical interaction between PCM and the dispersed NPs in PCM-nanocomposites Fig. 3 shows X-ray diffraction spectra of prepared TiO2 NPs (curve a), pristine PCM (curve b) and PCM-TiO2 nanocomposites [curve (c) and (d)] samples with 0.2 and 1 wt.% TiO2 nanoparticles. The XRD pattern of pure Mg(NO3)2•6H2O (curve b) with predominant peaks at 15.5°, 27.4°, 30.9°, and are in well agreement with reported literature . The diffraction peaks of TiO2 nanoparticles at 25.44°, 36.16°, 47.91° 54.43°, and 63.4° indicate anatase phase formation is also in good agreement with the reported literature [28]. The XRD pattern (Fig. 3 curve (c and d) of PCM nanocomposite depicts peaks of both TiO2 NPs and pristine PCM. This confirms that the crystalline phase of Pristine PCM is not affected by the addition of TiO2 NPs. The XRD spectrum of PCM-ZnO, PCM-Fe2O3, and PCM-SiO2 nanocomposite is also shown in Fig. S5(a-c) and depicting similar behavior as demonstrated by the spectra of PCM-TiO2 nanocomposite. Hence, the above characterizations confirm the formation of uniform PCM-nanocomposites without any chemical integration between pristine PCM and all respective nanoparticles.

Heat transfer characteristics

The thermal energy transfer characteristics of pristine PCM and PCM nanocomposites were evaluated by comparing their melting (charging) and solidification (discharging) cycles with the help of the conventional heating system. represents the melting cycles of pristine PCM and PCM nanocomposite with increasing concentration of TiO2 nanoparticle from 0.2–1 wt.% at the heating rate of 5 °C/ minute. At the beginning of the melting cycle, both pristine PCM and PCM nanocomposite were at the ambient temperature. The melting time of the PCM-TiO2 nanocomposites is shown in the inset image of indicates that solid pristine PCM is taking 49 min for initiation of melting phenomena. On increasing concentration of TiO2 NPs from 0.2 wt.%, 0.5 wt.% to 1 wt.% in pristine PCM, a continuous decrease in this melting time of PCM nanocomposites is observed. The maximum reduction of 38% in the melting time of PCM nanocomposite is observed for 1 wt.% TiO2 NPs embedded PCM-nanocomposites as compared to that of pristine PCM. Since the melting curve for 1 wt.% of TiO2 NPs in PCM show negligible detection of phase transition at a heating rate of 5 °C/minute. Therefore another melting cycle with a low heating rate of 2 °C/minute was performed and confirms the phase transition of PCM nanocomposite shown in Fig. S6. Our reported results are quite good and show improvement in comparison to the previously reported results in the literature , which shows a reduction in the melting time of paraffin by 33.3% with the addition of 1 wt.% Cu NPs. Our results are also in agreement with the study of Frusteri et al. showing simulated phase change of inorganic PCM containing with different wt.% carbon fibers. The solidification curves on PCM and PCM-TiO2 nanocomposites were also performed by using a conventional heating system and the results are shown in . At the initial stage of the solidification process, the temperature of pristine PCM and PCM nanocomposite are found to be at 120 °C. After allowing both the materials to cool

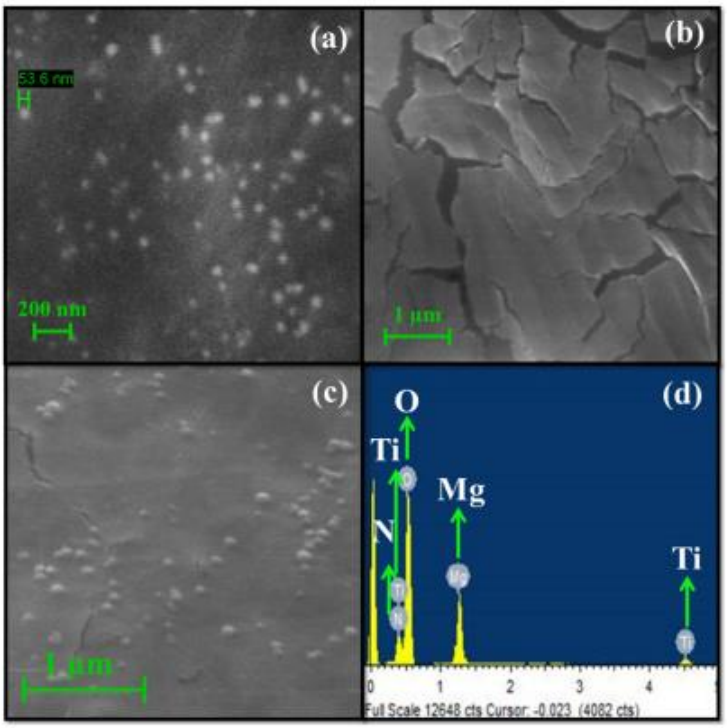

Fig. 1. SEM micrograph of (a) TiO2 Nanoparticles, (b) pristine PCM, (c) PCM-TiO2 nanocomposite and (d) EDX Spectrum of PCM- TiO2 nanocomposite.

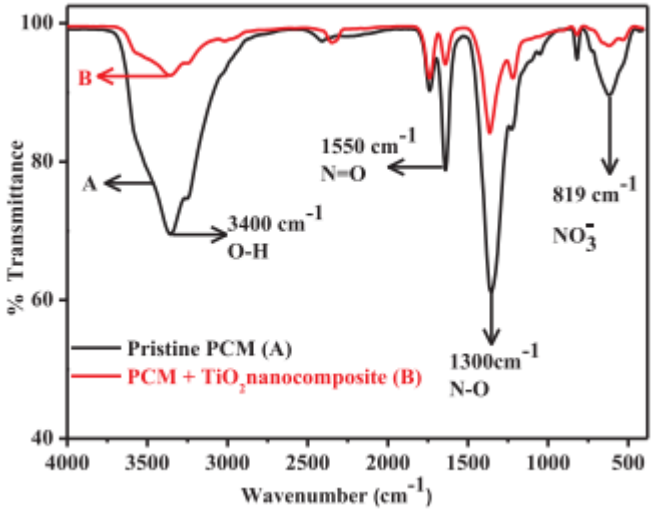

Fig. 2. FTIR spectra of Pristine PCM (curve A) and PCM-TiO2 nanocomposite (curve B).

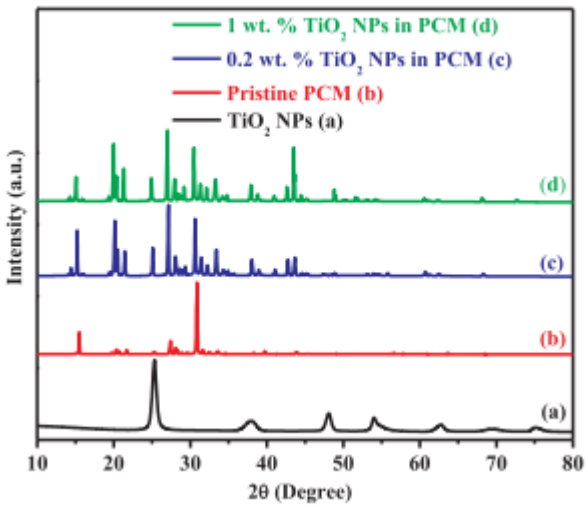

Fig. 3. XRD spectra of TiO2 NPs (curve a), PCM (curve b) and PCM –TiO2 nanocomposite with 0.2 and 1 wt.% TiO2 NPs (curve c and d).

naturally, the temperature of the pristine PCM and PCM nanocomposite decreases until it reached its solidification point. The solidification time of the PCM-TiO2 nanocomposites curves shows similar behavior like melting curve, i.e. the solidification time decreases with increasing concentration of TiO2 nanoparticle from 0.2–1 wt.% as shown in the inset image of Fig. 5. It is observed that the solidification time of PCM nanocomposite for 1 wt.% is reducing significantly by 77.5% compared to that of pristine PCM. Our reduction in solidification time of PCM nanocomposites also shows improvement in comparison to the reported results where the addition of 1 wt.% Cu nanoparticles into paraffin lead to 31.6% reduction in the solidification time. Liu et al. also reported a reduction of 28.5% in the freezing time of BaCl2/H2O solution with the addition of 1.13 vol% of TiO2 nanoparticles. The reduction in melting and solidification times of PCM-nanocomposites clearly indicates that the thermal conductivity of PCM is significantly enhanced by the addition of TiO2 NPs in PCM matrix. This enhancement can be attributed to the higher thermal conductive network of TiO2 nanoparticles as fillers and providing a lower resistance path for phonon transportation. The above results confirm that our composite exhibit improvement in heat transfer rate, and can be useful in thermal energy storage application. The melting and solidification curves of other PCM-metal oxides (ZnO, Fe2O3, and SiO2) are also shown in Fig. S7(a-c) and Fig. S8(a-c). The enhancement in melting and solidification rate of ZnO, Fe2O3, and SiO2 NPs embedded PCM nanocomposite are 8.5%, 7.4%, 6.3%, and 40%, 50%, 35%, respectively, in comparison to the pristine PCM. These results imply that TiO2 NPs embedded PCM nanocomposite show relatively better heat transfer characteristics.

Thermal conductivity analysis

Thermal conductivity is an important parameter for selecting PCMs for the thermal energy storage application . In nanocomposite, the heat transfer occurs by electron and phonons (vibrating with different frequencies particles). These acoustic phonons with different frequencies play a very important role in the thermal conductivity, while electronic contribution is almost negligible . In nanocomposites, heat is transferred within the matrix through phonons from one particle to another. The main aim of this work is to analyze the change in thermal conductivity due to the dispersion of highly conductive metal oxide nanoparticles in inorganic salt hydrate PCMs. Fig. 6(a) and Table 1 depict the thermal conductivity at room

temperature between pristine PCM (Magnesium nitrate hexahydrate) and it's composite with various wt.% of TiO2 metal oxides NPs. The results displayed that the maximum enhancement in thermal conductivity is 162.5% at 1 wt.% of TiO2 nanoparticles in PCM. This enhancement can be attributed to the role of TiO2 nanoparticles as fillers in PCM matrix. The addition of high conductive nanoparticles in the PCM matrix forms the high thermal percolation network, which allows the transportation of phonons very efficiently which leads to enhances thermal conductivity . The enhancement rate in thermal conductivity with respect to added wt.% from 0.2 wt.% to 0.5 wt.% of TiO2 NPs in pristine is more as compared to 0.5 wt.% to 1 wt.%. This change in thermal conductivity with respect to wt.% can be attributed to the presence of an inherent threshold value of thermal resistance of TiO2 NPs as filler at the interface of PCM and nanoparticle. The high thermal resistance across the interface associated with acoustic phonons, limit the heat transfer between the nanoparticles within a percolation network . The thermal conductivity of pristine PCM with metal oxides nanoparticles such as SiO2, ZnO, Fe2O3, and TiO2 as fillers at mass fraction of 0.5 wt.% are shown in Fig. 6(b) and Table 2. The results display that the thermal conductivity of PCM with other metal oxides (SiO2, ZnO, Fe2O3 and TiO2) constituting PCM nanocomposite are 0.56, 0.58, 0.62, 0.65 and 0.9 W.m−1.K−1 respectively, correspond to% improvement of 45, 55, 62.5 and 147.5% respectively. These results indicate that the TiO2 nanoparticle enhances maximum thermal conductivity amongst all other metal oxides NPs because of its high surface area and less agglomeration in the composite, also provide the lesser interfacial thermal resistance across the interface which help in better heat transfer within the percolation network as compare to other NPs.

Thermal properties

DSC analysis was carried out to investigate the effect of nanoparticles on the thermophysical properties of PCM. The DSC curve of the Pristine PCM is shown in Fig. 7(a), depicts the endothermic and exothermic peaks. It confirms the melting transition temperature (Tm) and solidification transition temperature (Tc) as 91.5 and 66.45 °C respectively. The latent of heats of fusion (Hm) and solidification (Hs) are 146 KJ.Kg−1 and 138 KJ.Kg−1 respectively. The transition point Tc shows the supercooling effect and can be measured by the degree of supercooling (Δ Ts) which is the difference between two transition temperature i.e. ΔTs =Tm-Tc Fig. 7(b) shows the DSC curve of the PCM-TiO2 nanocomposite with an increasing concentration of TiO2 nanoparticle from 0.2–1 wt.%. The measured latent heat from the DSC curve for the 0.2 wt.%, 0.5 wt.%, and 1 wt.% of PCM-TiO2 nanocomposites is found to be 137, 134, and 134.4 KJ.Kg−1 for melting and 135, 133, and 134 KJ.Kg−1 for freezing cycles. An overall reduction by 6.16%, 8.21%, and 7.80% for melting and 2.2%, 3.6%, and 2.6% for freezing is observed with respect to pristine PCM. Thus the latent heat of PCM-TiO2 nanocomposites decreases with increase the mass fraction of nanoparticles up to 0.5 wt.% and afterward negligible change is observed with an increase of wt.% of TiO2 nanoparticles in pristine PCM. The observed degree of supercooling `was found to be 6.9, 7.7, and 6.8 for 0.2 wt.%, 0.5 wt.%, and 1 wt.% of TiO2 NPs respectively in PCM-TiO2 nanocomposites. The addition of TiO2 nanoparticles is reducing the degree of supercooling which can be attributed to embedded nanoparticles in PCM matrix, which are acting as nucleation agents to facilities the crystallization of PCM. The thermal properties extracted from the DSC curve Fig. 7(b) are also summarized in table 3. The increase in wt.% of metal, metal oxide, the carbon in Pristine PCM leads to increase thermal conductivity of PCM-nanocomposites up to a certain wt.% . However, on further increasing concentration, the latent heat of PCM nanocomposite deteriorates because of the addition of nanoparticles that are not taking participation in latent heat storage . Therefore the optimum concentration of highly conducting NPs is required to exploit better thermophysical properties

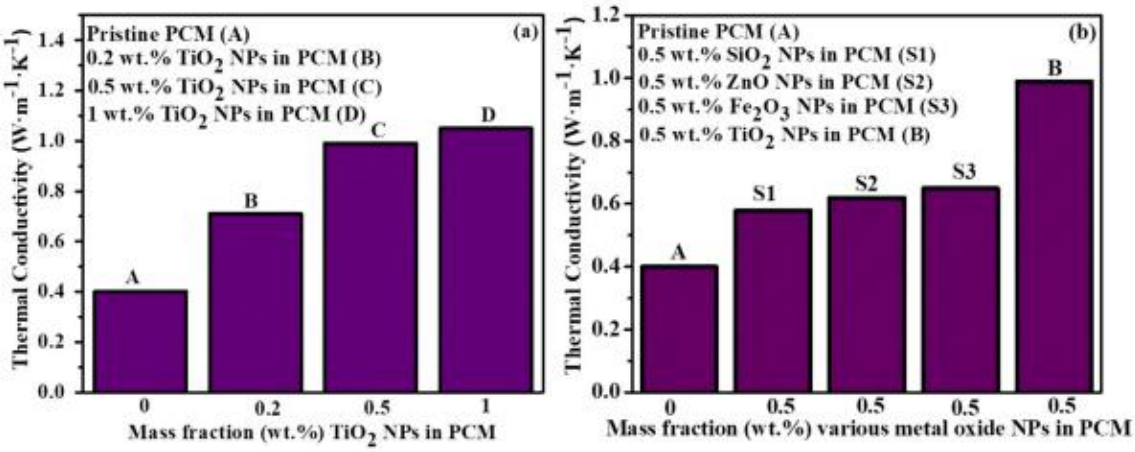

Fig. 6. Thermal conductivity of (a) pristine PCM and PCM-TiO2 nanocomposite at different mass fractions (0.2–1) wt.% TiO2 NPs, (b) PCM-Metal oxides nanocomposite at mass fractions of 0.5 wt.% NPs.

Table 1 The thermal conductivity of PCM-TiO2 nanocomposites.

S. No	Composite	wt.% of TiO2 NPs	W.m−1.K−1	Improvement (%)
1	PCM	0	0.4	–
2	PCM-TiO2	0.2	0.71	77.5
3	PCM-TiO2	0.5	0.99	147.5
4	PCM-TiO2	1	1.05	162.5

Table 2 The thermal conductivity of PCM- Metal oxide nanoparticles composites at mass fraction of 0.5 wt.% nanoparticles.

S. No	Composite	wt.% of MOx NPs	W.m−1.K−1	Improvement (%)
1	PCM-ZnO	0.5	0.58	45

2	PCM-Fe2O3	0.5	0.62	55
3	PCM-SiO2	0.5	0.65	62.5
4	PCM-TiO2	0.5	0.99	147.5

of so formed PCM nanocomposites. In this work other metal oxide nanoparticles such as ZnO, Fe2O3 and SiO2 are chosen with 0.5 wt.% in PCM matrix to form the PCM-metal oxide nanocomposites and their DSC curve are shown in Fig. S9(a-c). Similar to the PCM-TiO2 nanocomposite, the addition of these nanoparticles also influence the latent heat of composites. The measured latent heat of pristine PCM (Hm).

Table 3 Thermal properties for PCM and PCM-MOx nanocomposites at different mass fraction

S. No	Samples	wt. % of	Tm (°C)	*Hm	Tc(°C)	*HC	#Δ Ts/
		NPs					°C)
1	Pristine PCM	0	91.5	146	66.45	138	25.05
2	PCM-TiO2	0.2	91.9	137	85	135	6.9
3	PCM-TiO2	0.5	91.8	134	84.1	133	7.7
4	PCM-TiO2	1	91.3	134.6	85	134.4	6.8
5	PCM-ZnO	0.5	90.8	133.7	86.2	130.5	4.6

6	PCM-Fe2O3	0.5	90.9	130.9	84.5	120	6.4
7	PCM-SiO2	0.5	90.9	135.6	85.6	128.1	5.3

drops from 146 KJ.Kg−1 to 133.7, 130.9, 135.5 KJ.Kg−1 for melting and latent of solidification decreases from 138 KJ.Kg−1 to 133.7, 130.9, 135.6 KJ.Kg−1 for freezing cycles of ZnO, Fe2O3, and SiO2 nanoparticles based PCM-nanocomposites respectively. Thus the percentage reductions in latent heat are found to be 8.42, 10.3, 7.12 (for melting) and 5.4, 13.0, 7.17 (for freezing) to the ZnO, Fe2O3 and SiO2 based nanocomposites respectively. The degrees of supercooling are found to be 4.6, 6.4, and 5.3 for ZnO, Fe2O3, and SiO2 based nanocomposites. The thermal properties extracted from the DSC curve for these metal oxides nanoparticles Fig. S9(a-c) are summarized in table 3. These results showthat the metal oxide nanoparticles almost show similar effects in modifying the phase change properties of PCM. Our reported results also show improved thermophysical properties in comparison to the reported where the melting and freezing latent heat reduced by 12.14%, 13.03% and 5.9%, 6.7% for 0.5 wt.% of silver and copper nanoparticles with respect to pristine PCM.

CONCLUSION

This work presents a study on the improvement of the thermophysical properties of MOx NPs embedded PCM-nanocomposites. The PCM-Metal oxide nanocomposites are prepared by the melt mixing techniques. The SEM analysis shows that the as-prepared TiO2 nanoparticles possess spherical shape with an average particle size of 50 nm. The FTIR and XRD analysis confirm physical interaction among NPs and PCM material in PCM nanocomposites. The prepared nanocomposite exhibited a high heat transfer rate: the charging rate increased to 38% and discharging rate increased to 77.5% for 1 wt.% TiO2 NPs as compared to base PCM. The thermal conductivity of PCM-TiO2 nanocomposites increases with the increase in wt.% of TiO2 nanoparticles and maximum enhancement of 162.5% at 1 wt.% is achieved which is more than twice with respect to pristine PCM. This enhancement is less profound above the 0.5 wt.% TiO2 NPs as compared to that of 0.2 wt.% TiO2 NPs in PCM. This can be attributed to an increase in limiting interfacial thermal resistance between PCM and nanoparticles in PCM nanocomposites. Therefore, the optimal concentration of the nanoparticles to be dispersed in the PCM matrix is 0.5 wt.%. The% enhancement in thermal conductivity of the PCM-metal oxide (TiO2, SiO2, Fe2O3, and, ZnO) nanocomposites at 0.5 wt.% of nanoparticles are 147.5, 62.5, 55, and 45% which demonstrate that the TiO2 nanoparticle enhances the thermal conductivity in a larger extent than other metal oxides nanoparticles because of its high surface area and less agglomeration in the PCM matrix. The phase change properties of PCM-metal oxide nanocomposites measured by the DSC with respect to pristine PCM reveals that the addition of the nanoparticles maintains a high latent heat capacity of the material. The results show that the addition of nanoparticles also decreases the supercooling effect. The TGA results revealed that the PCM-metal oxide nanocomposites maintained their thermal and chemical stability. Finally, on the bases of instant solar water heating system results, it can be concluded that the PCM-metal oxides nanocomposites can be used as a promising candidate for the thermal energy storage application, due to its enhancement in thermal conductivity.

REFERENCES

1. T. Mahlia, T. Saktisahdan, A. Jannifar, M. Hasan, H. Matseelar, A review of available methods and development on energy storage; technology update, Renew. Sustain. Energy Rev. 33 (2014) 532–545.
2. M.M. Farid, A.M. Khudhair, S.A.K. Razack, S. Al-Hallaj, A review on phase change energy storage: materials and applications, Energy Conver. Manag, 45 (9–10) (2004) 1597–1615.
3. D.N. Nkwetta, F. Haghighat, Thermal energy storage with phase change material—A state-of-the art review, Sustain. Citie. Soc. 10 (2014) 87–100.
4. P. Zhang, X. Xiao, Z. Ma, A review of the composite phase change materials: fabrication, characterization, mathematical modeling and application to performance enhancement, Appl. Energy 165 (2016) 472–510.
5. C. Li, B. Zhang, B. Xie, X. Zhao, J. Chen, Z. Chen, Y. Long, Stearic acid/expanded graphite as a composite phase change thermal energy storage material for tankless solar water heater, Sustain. Citie. Soc. 44 (2019) 458–464.
6. F. Cheng, R. Wen, Z. Huang, M. Fang, Liu Yg, X. Wu, X. Min, Preparation and analysis of lightweight wall material with expanded graphite (EG)/paraffin composites for solar energy storage, Appl. Therm. Eng. 120 (2017) 107–114.
7. R. Wen, Z. Huang, Y. Huang, X. Zhang, X. Min, M. Fang, Liu Yg, X. Wu, Synthesis and characterization of lauric acid/expanded vermiculite as form-stabilized thermal energy storage materials, Energy Build. 116 (2016) 677–683.
8. B. Xu, H. Ma, Z. Lu, Z. Li, Paraffin/expanded vermiculite composite phase change material as aggregate for developing lightweight thermal energy storage cementbased composites, Appl. Energy 160 (2015) 358–367.
9. Z. Lu, J. Zhang, G. Sun, B. Xu, Z. Li, C. Gong, Effects of the form-stable expanded perlite/paraffin composite on cement manufactured by extrusion technique, Energy 82 (2015) 43–53.
10. Y.E. Milian, A. Gutierrez, M. Grageda, S. Ushak, A review on encapsulation techniques for inorganic phase change materials and the influence on their thermophysical properties, Renew. Sustain. Energy Rev. 73 (2017) 983–999.